

BIOMECHANICAL BREAST MODELING *State of the art*

Finite elements models are widely used to estimate body parts deformation under pre-defined boundary conditions. Several biomechanical models of the breast were recently developed providing physics-based predictions of tissue motion and internal stress and strain intensity.

In our work, we assume that the strain intensity obtained during the tissues deformation may be correlated with the patient discomfort. Thus, a biomechanical model obtained from the patient's MRI volume can be subsequently used to mimic breast compression during the mammographic acquisition. The resulting tissues strain cartography can be used as a first quantification of the patient inconfort.

This chapter provide theoretical background on continuous mechanic theory applied to soft tissues modeling. The principle of finite elements theory is defined including solid bodies and contact mechanics. A review of the existing biomechanical breast model is given describing the main challenges in the field and the proposed solution. These works provide the core foundation for the next developed patient specific breast model.

*our proposal
of a new*

are described,

680 2.1 Continuous mechanics

Continuous

Continuum mechanics is a branch of mechanics that deals with the analysis of the kinematics and the mechanical behavior of materials modeled as a continuous mass. Continuum mechanics is based on the continuum hypothesis: the matter is continuously distributed throughout the space occupied by the matter. The basis for the hypothesis is how physical quantities, as for example pressure, temperature, and velocity, are measured macroscopically.

Such as

In this section the continuous mechanis theory applied to solids ~~bodys~~ was described using the following sources: Belytschko et al. (2013); Abeyaratne (2012).

bodies

is

2.1.1 Deformation and strain

Then,

690 Continuous mechanics is the mathematical description of how physical objects ~~that occur~~ in nature respond to the application of forces.

A body is the mathematical abstraction of an object and is defined by its geometric and constitutive properties. At a macroscopic level, a solid object is described as homogeneous and continuous body, i.e. the substance of the object has a unique composition and completely fills the space it occupies thus, ignoring the granular (atomic) nature of matter. In continuous mechanics, a body \mathcal{B} is composed of particles p (or material points). Each particle is located at some defined point x in three dimensional space. The set of all the points in space, corresponding to the locations of all the particles, is the domain Ω occupied by the body in a given configuration, here also named geometry. A particular body can change its configuration and therefore the occupied region in the space when exposed to some external stimuli, like force, pressure or heat. *Such as* *response*.

The configuration of a body is defined as a one-to-one mapping between the particle p and position x , $\Omega_0 = \chi_0(\mathcal{B})$ (see figure 2.1). To describe the solid's response to external stimuli one needs to know the changes in geometrical characteristics between at least two configurations: the configuration that one wishes to analyze Ω_1 , and the reference configuration relative to which the changes are to be measured Ω_0 . Here, see figure 2.1, the mappings χ_0 and χ_1 take $p \rightarrow X$ and $p \rightarrow x$, thus X and x are the positions of particle p in the two configurations under consideration.

Frequently, the reference configuration is fixed for a given study and is chosen arbitrary in a the most convenient way among all the configurations that the body can sustain.

The deformation of the body from the reference configuration Ω_0 is characterized by the next defined mapping Φ :

$$x = \Phi(X) = \chi_1(\chi_0^{-1}(X)), \quad \text{where } X \in \Omega_0 \text{ and } x \in \Omega_1 \quad (2.1)$$

The displacement u of a particle is the difference between its position in the analyzed configuration (or current configuration) and its position in the reference configuration.

$$u(X) = \Phi(X) - X \quad (2.2)$$

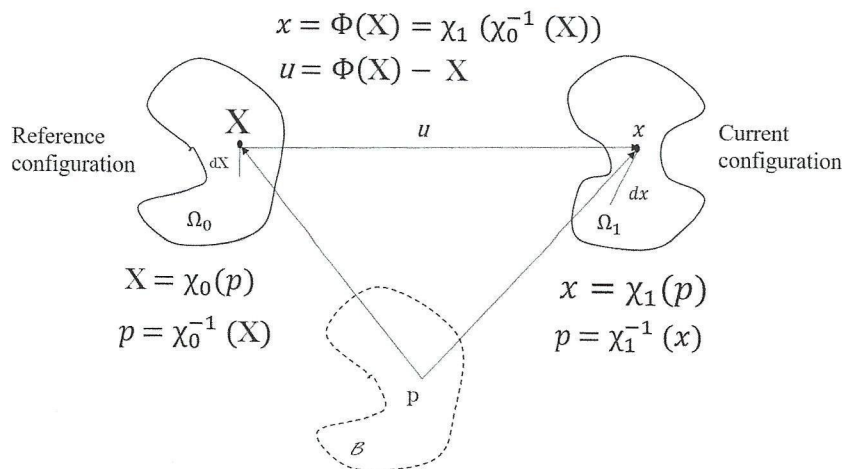


Figure 2.1: The position of a particle in the reference and current body configurations.

Suppose that $G(\Omega_1)$ is the value of some extensive physical property associated with the body \mathcal{B} in the current configuration (such as the body mass m). There exists a density $g(x)$ such that:

$$G(\Omega_1) = \int_{\Omega_1} g(x) dv$$

- ⁷¹⁵ where dv is the volume of the material element. Thus, the property $G(\Omega_1)$ is related to the body while the density $g(x)$ is related to the position of the body particle.

Eulerian and Lagrangian formulations

There are two classical techniques used to describe the body physical characteristics depending on the choice of independent variables. Some physical characteristics, such as mass density, can be defined for each individual particle. In such cases, the body characteristics are defined by the function :

$$\forall p \in \mathcal{B}, m = \mathcal{M}(p) \quad \text{a case,}$$

for all $p \in \mathcal{B}$. Here the coordinate system remains consistent and moves with the particle. Therefore, the coordinates of both the particle and the attached variable do not change along the deformation. A particle is an abstract entity and cannot be used in numerical calculations, thus it is described by its location in reference configuration $p = \chi_0^{-1}(X)$.

$$m = \mathcal{M}(p) = \mathcal{M}(\chi_0^{-1}(X))$$

We call X Lagrangian or material coordinates, and their application is called Lagrangian or material description.

Instead of defining body characteristics as a function of body particles, one can define directly as a function of particle location in current configuration by using the relation

[Pourquoi y a-t'il des équations
non linéaires ?]

$x = \chi_1(p)$, and therefore

$$m = \tilde{\mathcal{M}}(x) = \mathcal{M}(\chi_1^{-1}(x))$$

- 720 Here the coordinate system is fixed and the particle's coordinates are changing. Therefore, the position of particle and any related quantity changes during the deformation. We call x Eulerian or spatial coordinates and their application is called Eulerian or spatial description.

These approaches are distinguished by three important aspects: the mesh description, 725 the stress tensor and momentum equilibrium and the strain measure. The advantages and drawbacks of these two formulations will be discussed later in this chapter. Further, only Lagrangian formulation is used to describe the continuous deformation of soft tissues.

Deformation gradient

In mathematical formulation the deformation gradient tensor F is the Jacobian matrix of 730 the deformation $\Phi(X)$:

$$F = \frac{\partial \Phi(X)}{\partial X} = \frac{\partial x}{\partial X} \quad (2.3)$$

Considering infinitesimal quantities, the deformation gradient relates the segment dX in the reference configuration to the corresponding deformed segment dx in the current configuration (Figure 2.1)

$$dx = F \cdot dX. \quad (2.4)$$

In addition to the mapping of such vectors, the deformation gradient tensor allows also 735 the mapping of differential volumes as:

$$\int J \, dv = \det(F) dV = J dV \quad (2.5)$$

The Jacobian determinant of the deformation gradient tensor is a measure of the volume variation during the deformation. It can be used to relate extensive physical properties in the current and reference configurations:

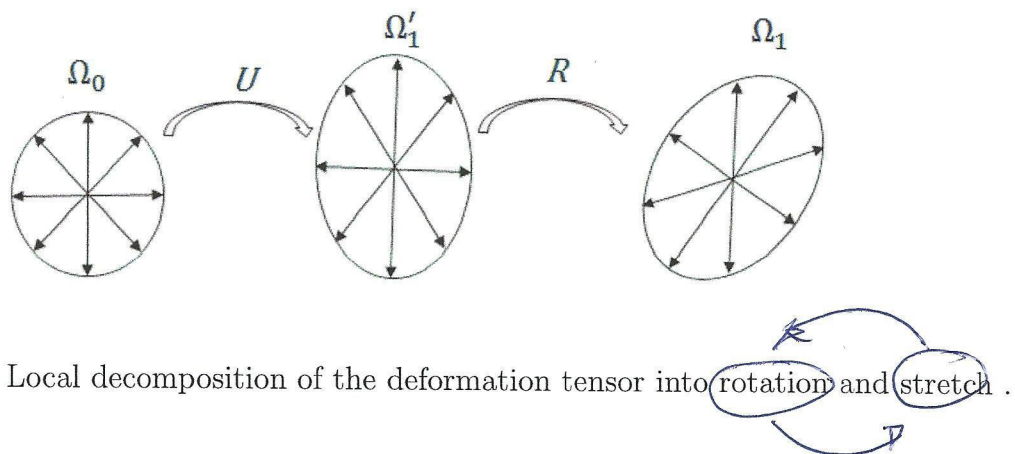
$$\int_{\Omega_1} g(x) \, dv = \int_{\Omega_0} g(\Phi(X)) J \, dV \quad (2.6)$$

Decomposition of the deformation gradient tensor into rotation and stretch

- 740 The deformation gradient tensor F completely characterizes the body deformation in the vicinity of a particle p . This deformation consists of a rigid body rotation and body stretch (see Figure 2.2). As dX and dx are differential segments, the map F is not affected by rigid-body translations.

Generally, the body stretch is defined as the ratio of the deformed line elements to the 745 length of the corresponding undeformed line element

$$l = \frac{|dx|}{|dX|}, \quad (2.7)$$



and consists locally on three mutually orthogonal stretches named **the principal stretches**.

According to the polar decomposition theorem, the deformation tensor can be written as the product of a proper orthogonal tensor R representing the rotational part, and a symmetric positive defined tensor U representing the body distortions.

$$F = R \cdot U. \quad \text{distortions} \quad (2.8)$$

where U and R are given by the relations $U = (F^T \cdot F)^{\frac{1}{2}}$ and $R = F \cdot U^{-1}$. The essential property of tensor U is that it is symmetric and positive, therefore it has three real positive eigenvalues $\lambda_1, \lambda_2, \lambda_3$ and a corresponding triplet of orthonormal eigenvectors r_1, r_2, r_3 . Thus then an infinitesimal segment dx is stretched by the tensor U , the segment is distorted in the principal directions of U by amounts of the corresponding eigenvalues of U .

The tensor U is also called the **right stretch tensor**. Since there is a one-to-one relation between U and U^2 , for the simplification of numerical calculus the stretch tensor can be replaced by the **Green deformation tensor** $C = F^T \cdot F$.

There are three particular functions of C called the **principal invariants**.

$$I_1(C) = \text{tr}C, \quad I_2(C) = \frac{1}{2} [\text{tr}C^2 - (\text{tr}C)^2], \quad I_3(C) = \det(C). \quad (2.9)$$

These functions are related to the three principal stretches by the next relations:

$$I_1(C) = \lambda_1^2 + \lambda_2^2 + \lambda_3^2, \quad I_2(C) = \lambda_1^2\lambda_2^2 + \lambda_2^2\lambda_3^2 + \lambda_3^2\lambda_1^2, \quad I_3(C) = \lambda_1^2\lambda_2^2\lambda_3^2 \quad \text{following} \quad (2.10)$$

The essential property of the principal invariants is that they don't change under coordinate transformations for a given body configuration. Their use to compute the body stretch will be an essential part of constitutive modeling, because the behavior of a material should not depend on the coordinate system.

It can be also shown that:

$$\det(C - \mu I) = -\mu^3 + I_1(C)\mu^2 - I_2(C)\mu + I_3(C) \quad (2.11)$$

Strain measures

Referring to small deformations, the engineering nominal strain is defined as the ratio of the change in length of the deformed line element to the length of the corresponding undeformed line element:

$$\epsilon = \frac{dx - dX}{dX} \quad (2.12)$$

When the body is not deformed, the deformation gradient F and therefore the right stretch tensor U is equal to identity tensor I . The strain in such a case is equal to zero.

For most biological soft tissues, large deformation has to be considered. In that case, the previously defined strain is no more applicable. For large deformations, a measure of strain can be any monotonically increasing function related to stretch in a one-to-one manner, *and* this function has to vanish in the reference configuration (?). In orthogonal coordinate system, an admissible function is

$$f(x) = \frac{1}{m}(x^m - 1) \text{ for } (m \in \mathbb{R}_{\neq 0}) \text{ and } \ln(x) \text{ for } (m = 0) \quad (2.13)$$

For $m = 0$ the function represents the Hencky strain tensor,

$$E = \ln(U), \quad (2.14)$$

for $m = 1$ the function represents the Biot strain tensor

$$\text{this function represents } E = U - I, \quad (2.15)$$

and for $m = 2$ the Green-Lagrangian strain tensor:

$$E = \frac{1}{2}(U^2 - I) = \frac{1}{2}(C - I) \quad (2.16)$$

The Green-Lagrangian tensor is commonly used in practice as, by using the relation 2.11, it can be computed without prior knowledge of the eigenvectors of the Green deformation tensor C .

2.1.2 Stress measures

Generally, forces are categorized as internal and external forces. An **external force** is a force caused by an external agent outside of the system, and contrariwise an **internal force** is a force exchanged by the particle in the system. The external forces, in turn, are categorized in **body forces** (acting at the distance) and **contact forces** (acting on the body surface). The relation between body forces per unit undeformed volume $\tilde{b}(X)$ (Lagrangian coordinates) and body forces per unit deformed volume $b(x)$ is given by the following relation:

$$\tilde{b} = \frac{dv}{dV} b = Jb. \quad (2.17)$$

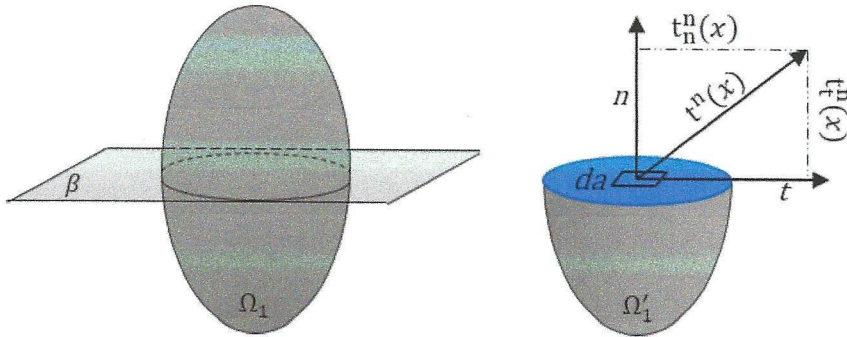


Figure 2.3: True stress vector $t^n(x)$ at point x on the fictitious surface created by the cutting plane β of normal \vec{n} passing through the point x .

The contact forces can act on the external surface of the body or on a imaginary internal surface enclosing a volume element (Fig. 2.3). In general terms, the stress (or the **traction vector**) $t^n(x)$ is defined as contact force per unit area da in the limit as $da \rightarrow 0$. Therefore $t^n(x)$ varies from point to point in intensity and orientation depending on the $da(n)$ orientation. The stress vector projection on normal axis n defines the **normal stress vector** and its projection on the tangential axis define the **shear stress vector**.

The stress on the boundary $\partial\Omega_1$ of the region occupied by the body is applied by external forces through physical contacts along the boundary. When formulating and solving a boundary-value problem, this stress defines the boundary conditions.

800 Cauchy's lemma

Cauchy's lemma states that traction vectors acting on opposite sides of a surface are equal and opposite.

$$t^{-n}(x) = -t^n(x) \quad (2.18)$$

Cauchy's Law

Cauchy's law states that there exists a Cauchy stress tensor σ which maps linearly the normal to a surface to the stress vector acting on that surface, according to the next relation

$$t^n = \sigma \cdot n \quad \text{where} \quad t_i^n = \sigma_{ij} n_j \quad (2.19)$$

When large deformations are considered, the reference and current configurations of the body are significantly different and a clear distinction has to be made between them. The traction vector t^n is defined in Eulerian coordinates (body current configuration) and is also called the **true stress**. Accordingly, the Cauchy stress tensor σ is called the true stress tensor.

The definition of any measure with respect to the deformed configuration is less practical as it is usually unknown a priori. For the simplification of mathematical formulation, a

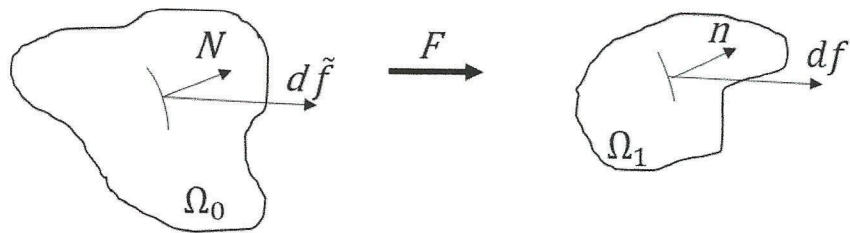


Figure 2.4: Deformation of area dA into area da . The force df acting on deformed area da and the pseudoforce $d\tilde{f}$ acting on undeformed area dA

new pseudostress is defined in the Lagrangian coordinate space named the **engineering stress**. The engineering stress has no physical meaning and has to be converted into true stress for any interpretations.

~~Below~~ Next, two ~~pseudostress~~ vectors are defined (Fig. 2.4):

- T^N defined as the contact force df per unit area dA in reference configuration.
- \tilde{T}^N defined as the contact pseudoforce $d\tilde{f}$ per unit area dA in reference configuration.

Accordingly, two pseudostress tensors are defined based on pseudostress vectors:

- $T^N = P \cdot N$, P is called **first Piola-Kirchhoff stress tensor**,
- $\tilde{T}^N = S \cdot N$, S is called **second Piola-Kirchhoff stress tensor**.

Kirchhoff

where N is the normal vector of unit area dA in the reference configuration.

The three stress tensors are linked by the next relation

$$\sigma = J^{-1} F \cdot P = J^{-1} F \cdot S \cdot F^T \quad (2.20)$$

2.1.3 Conservation equations

Three conservation laws must be satisfied by physical system subject to any applied boundary conditions: **conservation of mass**, **conservation of linear momentum** and **conservation of angular momentum**. The resulting equations describe partially the mechanical behavior of a continuous body.

Conservation of mass

The mass m of a body with the density ρ , that infills the space region Ω_1 is given by :

$$m(\Omega) = \int_{\Omega} \rho(X) dV \quad (2.21)$$

The mass conservation law requires that the body mass remains constant throughout all possible body configurations. For a Lagrangian formulation, this results in a relation

between the body density in the reference configuration ρ_1 and the body density in the current configuration ρ .

$$2.5 \quad \int_{\Omega_1} \rho_1 dv = \int_{\Omega_0} \rho_0 dV = \text{const.} \quad \leftarrow (\text{numerotation?})$$

Using the relation 2.6 one can deduce that:

$$\int_{\Omega_0} (\rho_1 J - \rho_0) dv = 0 \quad \text{and} \quad \rho_1 J = \rho_0 \quad (2.22)$$

Conservation of the linear momentum

~~Let assume~~ Assume that a body B is defined on a arbitrary region Ω_0 with boundary Γ_0 , and is subjected to a body-force $\rho_0 b$ and the surface traction T^N . And let X be the particle location in the undeformed solid. The total force acting on the body B is defined as:

$$f = \int_{\Omega_1} \rho_0 b(X) dV + \int_{\Gamma_0} T^N(X) dA \quad (2.23)$$

The conservation of the linear momentum requires that the total force f acting on the body to be equal to the time rate change of the linear momentum. In a static problem the time rate change of the linear momentum is neglected and thus an equilibrium equation is obtained.

$$\cancel{\text{the}} \quad \rho_0 b + \nabla_0 \cdot P = 0 \quad (2.24)$$

Where the P_{ji} are the components of first Piola-Kirchhoff stress tensor. The equilibrium equation can be formulated in terms of the second Piola-Kirchhoff stress tensor by using ~~the~~ relations 2.20.

Conservation of angular momentum

~~The~~ The conservation of angular momentum requires that the resultant momentum on any part of the body about a fixed point O equals the rate of increasing of its angular momentum (about O). For a static problem, the integral form of the conservation of angular momentum is defined as:

$$\int_{\Omega_0} X \times \rho_0 b(X) dV + \int_{\partial\Omega_0} X \times T^N(X) dA = 0 \quad (2.25)$$

The relation 2.25 requires that the second Piola-Kirchhoff stress tensor is a symmetric tensor:

$$S = S^T \quad (2.26)$$

In summary, the conservation equations are fulfilled if and only if the following local conditions are fulfilled at each point in the body:

$$\rho_1 J = \rho_0, \quad \nabla_0 \cdot S \cdot F^T + \rho_0 b = 0, \quad S = S^T \quad (2.27)$$

with the traction on the surface related to the stress through $\tilde{T}^n = S \cdot N$. For the simplification of mathematical calculus, the constitutive equations are formulated in terms of the second Piola-Kirchhoff stress tensor using the relations 2.20.

2.1.4 Constitutive models

The constitutive models, called also material models, define the relation between stress and strain of a physical system under the action of external stimuli. It is almost impossible to define a universal material behavior capable to model the material response to all possible conditions. Thus, for a given material, several constitutive models can be defined depending on the studied characteristics.

Biological materials are classified into:

- *Isotropic or anisotropic materials*: in a isotropic (anisotropic) material the values of a property ~~is constant (vary)~~ with respect to the direction.
- *Compressible or incompressible materials*: in a compressible (incompressible) material the volume changes (~~remains constant~~) during the deformation and the density remains constant. For a incompressible material the Jacobian determinant of the deformation tensor J is equal to 1.
- *Homogeneous or heterogeneous materials*: in a homogeneous (heterogeneous) material the values of a property ~~is constant (vary)~~ with respect to the position within the body.

Biological soft tissues are modeled using elastic materials model. The elasticity is the property of a solid material to return to its original size and shape when the influence of an external force is removed. In this case the strains are said to be reversible.

Considering small deformations, the stress-strain law of a linear material is given by the **Hook's law**

where the coefficient of proportionality λ is named **Young's modulus**.

Elastic materials may be defined ~~also~~ with a non-linear stress-strain relationship. In such cases the elastic moduli (λ) is defined ~~is~~ function of strain ϵ

$$\lambda = \frac{\partial \sigma}{\partial \epsilon} = f(\epsilon).$$

For example, for an elastic exponential material (Azar et al., 2002) the elastic moduli is computed using the function

$$f(\epsilon) = b e^{m\epsilon}, \quad (2.28)$$

where b and m are material parameters.

For large deformation the stress-strain relationship is deduced from a potential function. A **hyperelastic** material is an elastic material for which the work is independent of the deformation path. The material reversibility and path-independent behavior implies the absence of energy dissipation during the deformation. Thus there exists a potential function $W(E)$ such that

$$S = \frac{\partial W(E)}{\partial E} = 2 \frac{\partial \psi(C)}{\partial C}$$

Il faut définir ψ .
Par ailleurs, je suppose que
 E est le strain tensor et que
 C est le Green deformation tensor.

Draft

[Modulus \rightarrow singulier]
[Modulus \rightarrow planel]

(strain related to deformation at constant volume)

- 880 Moreover, if the material is isotropic, the stored strain energy W of a hyperelastic material can be written as a function of principal invariants (I_1, I_2, I_3) of the Green deformation tensor C previously defined in equation 2.9.

We introduce below the most used potential functions for the characterization of biological soft tissues.

- 885 For the simplification of potential expressions, we define the first and the second deviatoric strain invariants:

$$\bar{I}_1 = \frac{I_1}{I_3^{2/3}}; \quad \bar{I}_2 = \frac{I_2}{I_3^{4/3}}$$

- We also define the **Bulk modulus** as measure of a material's resistance to compression, the **shear moduli** as the ratio of shear stress to the shear strain and the **Poisson ratio** as the ratio between longitudinal strain to the transverse strain describing the body shape change. For small deformation the Bulk modulus and shear moduli are linked to the Young's modulus and Poisson ratio by the next relations:

$$K = \frac{\lambda}{3(1-2\nu)} \quad \text{and} \quad \mu = \frac{\lambda}{2(1+\nu)} \quad (2.29)$$

Neo-Hookean potential function

- The Neo-Hookean (Treloar, 1943) law is an extension of the Hook's law to large deformations. The potential function is based only on the first invariant and is given by

$$W = \frac{\mu}{2}(\bar{I}_1 - 3) + \frac{K}{2}(J - 1)^2, \quad (2.30)$$

where μ and K are initial shear moduli and initial Bulk modulus respectively.

Mooney-Rivlin potential function

The potential function of a Mooney-Rivlin (Rivlin and Saunders, 1951) material can be defined as:

$$W = \frac{\mu_1}{2}(\bar{I}_1 - 3) + \frac{\mu_2}{2}(\bar{I}_2 - 3) + \frac{K}{2}(J - 2)^2, \quad (2.31)$$

- 900 where the constants μ_1 and μ_2 describing the material properties are linked to the initial shear moduli $\mu = (\mu_1 + \mu_2)$, and the constant K is the initial Bulk modulus.

Gent potential function

The potential function of a Gent (Gent and Thomas, 1958) material model is defined as:

$$W = -\frac{\mu J_m}{2} \ln \left(1 - \frac{\bar{I}_1 - 3}{J_m} \right) + \frac{K}{2} \left(\frac{J^2 - 1}{2} - \ln J \right), \quad (2.32)$$

- 905 where μ and K are the initial shear moduli and the initial Bulk modulus respectively. And J_m is a parameter limiting the value of $(\bar{I}_1 - 3)$.

Ogden model

The Ogden (Ogden, 1972) material model is based on the three principal stretches ($\lambda_1, \lambda_2, \lambda_3$) and $2N$ material constants, where N is the number of polynomials that constitute the potential function:

$$W = \sum_{i=1}^N \frac{\mu_i}{\alpha_i} (\lambda_1^{\alpha_i} + \lambda_2^{\alpha_i} + \lambda_3^{\alpha_i} - 3) + \sum_{k=1}^N \frac{K}{2} (J - 1)^{2k}, \quad (2.33)$$

where μ_i and α_i are material constants, and K is the Bulk modulus.

Yeoh model

The potential function of Yeoh (Yeoh, 1990) model is based on the first invariant:

$$W = \sum_{i=1}^N \mu_i (\bar{I}_1 - 3)^i + \sum_{k=1}^N \frac{K}{2} (J - 1)^{2k}, \quad (2.34)$$

where the μ_i are material constants and K is the Bulk modulus.

Governing equations of Lagrangian formulation

We consider a body \mathcal{B} which occupies in the reference configuration the domain Ω_0 with a boundary Γ_0 . The governing equations for the mechanical behavior of a continuous body are:

1. Conservation of mass $\rho_1 J = \rho_0$
2. Conservation of linear momentum $\nabla \cdot P + \rho b = 0$
3. Conservation of angular momentum $F \cdot P = P^T \cdot F^T$
4. Constitutive equations
5. Measure of strain $E = \frac{1}{2}(C - I)$
6. Boundary condition: $e_i \cdot N \cdot P = e_i \cdot \bar{t}$ on $\Gamma_0^{t_i}$
7. Internal continuity condition: $[e_i \cdot N \cdot P] = 0$ on Γ_0^{int}

Where we note $\Gamma_0^{t_i}$ the set of prescribed traction \bar{t} on the body boundary Γ_0 ; and Γ_0^{int} is the union of all surfaces where the stresses are discontinuous in the body (material interfaces).

The momentum equation together with the traction boundary condition and interior traction continuity condition are called generalized momentum balance (GMB).

930 2.2 Finite Element Discretization

In continuous mechanics the body deformation is expressed in terms of partial differential equations (PDEs). For the majority of problems, the PDEs cannot be solved analytically, therefore approximation methods are developed. To this end, the finite element (FE) method has become the standard numerical calculation to compute such approximations.
 935 The computational domain, the unknown solution, and its partial derivatives are discretized, so as to obtain a set of algebraic equations for the function values at a finite number of discrete locations. The unknowns of the discrete problem are associated with a computational mesh which represents a subdivision of the domain Ω_0 into many small control volumes Ω_k .

940 2.2.1 Eulerian and Lagrangian mesh description

The mesh description depends on the chosen independent variables (Eulerian or Lagrangian formulation). An Eulerian mesh formulation is usually used to solve problems linked to fluid like materials and a Lagrangian mesh for solid like materials. In an Eulerian mesh, the Eulerian coordinates of nodes are fixed (coincident with spatial points) and the material points change in time (see Figure 2.5.b). In this case the mesh has to be large enough to contain the body in its current configuration. Throughout the deformation, the material points will belong to different elements. On the contrary, in a Lagrangian mesh, the Lagrangian coordinates of nodes are time invariant, nodal trajectory corresponds with material points trajectory and no material passes between elements (see Figure 2.5.a).

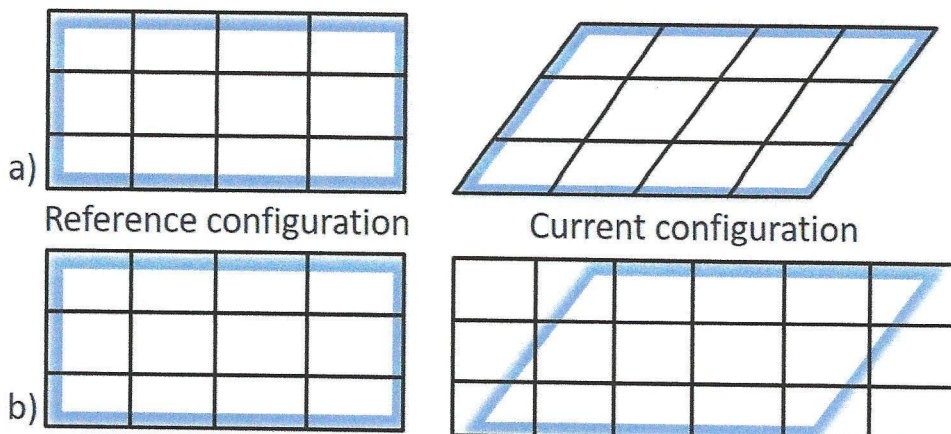


Figure 2.5: a) Lagrangian mesh formulation. b) Euler mesh formulation

950 In a Lagrangian mesh, the boundary and interface nodes remain coincident with body boundaries and material interfaces throughout the entire deformation. Thus, the boundary conditions are defined directly on the respective nodes. On the other hand, in an Eulerian mesh, the boundary and interface conditions have to be defined on points which are not nodes. This implies important complications in multi-dimensional problems.

955 An important drawback of a Lagrangian mesh affect mainly the large deformation domain. As the nodes are coincident with the material points, the elements deform with materials. Therefore, the magnitude of deformation is limited because of element distortion. The limited distortion that most elements can sustain without performance degradation or failure is an important factor in nonlinear analysis with Lagrangian formulation.

960 2.2.2 Lagrangian mesh

The general approach of the FE method in Lagrangian formulation is shown in Fig. 2.6. First, the momentum equations with given boundary conditions are multiplied by a set of appropriate test functions. The test functions have to satisfy all displacement boundary conditions and to be smooth enough so that all derivatives in momentum equations are well defined. Then, performing an integration by parts, the weak formulation of GMB is obtained, also called the principle of virtual work (Belytschko et al., 2013).

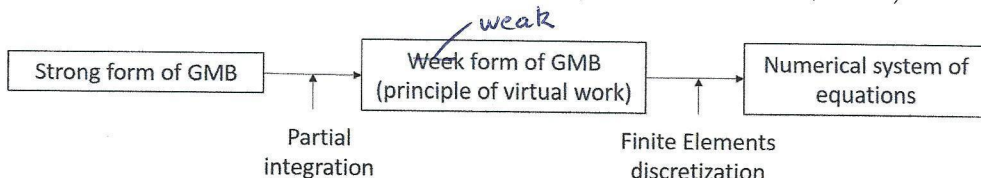


Figure 2.6: From strong formulation of the generalized momentum balance (GMB) to numerical equations.

The momentum equations and the traction boundary conditions, usually called the strong form, cannot be directly discretized by FE method. The strong formulation of the GMB equations impose the C_1 continuity conditions on the field variables. Therefore, the solution of this problem does not always exist. This is true especially in the case of complex domains with different material interfaces. In order to overcome these difficulties, weak formulations are preferred. The weak formulation of GMB reduces the continuity requirements thereby allowing the use of easy-to-construct and implement polynomials. Because of the reduction in the requirements of function smoothness, the weak forms never give an exact solution, but one can obtain a relatively accurate solution with the discretization refinement.

From the weak form of the GMB equations, the numerical system of equations is formulated by using finite elements interpolants for the mechanical displacement and the test functions. The whole domain is discretized into a number of smaller areas or volumes which are called **finite elements** and their assembly is called a **mesh**. Elements can be of various shapes (as shown in Figure 2.7.b), quadrilateral or triangular in two dimensions, and tetrahedral or hexahedron in three-dimensions.

The mechanical displacement is approximated at the discretization points called finite element **nodes**. The nodes are at the vertices of the elements for a linear type, and at the vertices and midsides of the edges for a quadratic type (figure 2.7.b). The displacement of each point within an element is interpolated from the values of the displace-

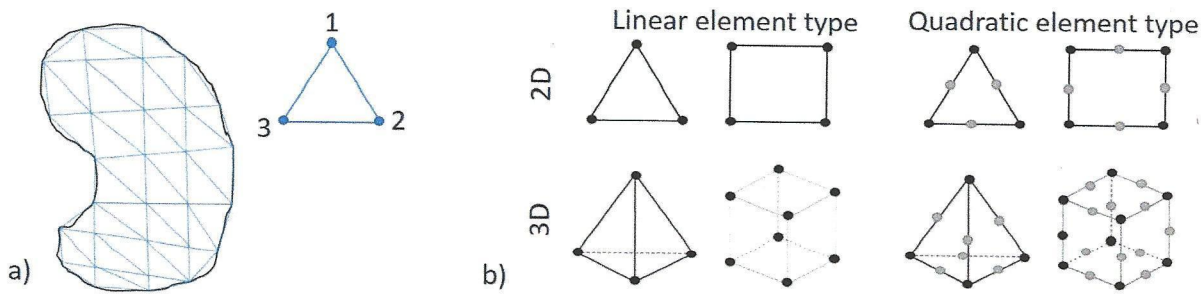


Figure 2.7: a) Discretization of a 2D domain with triangular finite elements :Lagrangian mesh . b) Different types of finite elements

ments of the nodes of ~~this~~ element. In this way, the problem of finding the displacement of every point within the body is replaced by the problem of finding the displacements of a finite number of nodes.

As in a Lagrangian mesh the nodes are following the motions, for large deformation ~~the~~ the finite elements can be highly distorted. Therefore, the element's shape quality is generally checked all along the deformation process. Several shape parameters for each element type have been proposed ~~such as~~ such as: aspect ratio, maximum corner angle, Jacobian ratio, skewness, parallel deviation, warping factor. The acceptable limit values of these shape factors are proper to the element ~~types~~ types.

In the following, only the shape parameters of the linear triangular elements are presented (ANSYS, 2017b).

~~the~~ Triangle aspect ratio

The element's shape aspect ratio is computed using only the vertex ~~corner~~ corner nodes of the element (Figure 2.8). First, two lines are created: one through a node (K) and the midpoint of the opposite edge (K'), the second through the midpoint of the other two edges (J' and I'). Then two rectangles are created, each rectangle ~~have~~ having a pair of edges parallel to one of previously defined lines. The rectangle edges have to pass through the nodes and the triangle's edges' midpoints. This construction is repeated for each triangle's node resulting in 6 rectangles. The aspect ratio of a rectangle is defined as the ratio between the longer and shorter side. Thus, the triangle's aspect ratio is defined as the maximal aspect ratio over the 6 rectangles divided by squared root of 3.

The best possible aspect ratio is 1 and is represented by an equilateral triangle. An element with an aspect ratio larger than 20 is considered as bad aspect element, large aspect ratio may degrade solution performance.

Triangle maximum corner angle

The maximum corner angle is computed using nodes position in 3D space. The best possible maximum corner angle is 60° . An element having a maximal corner angle larger

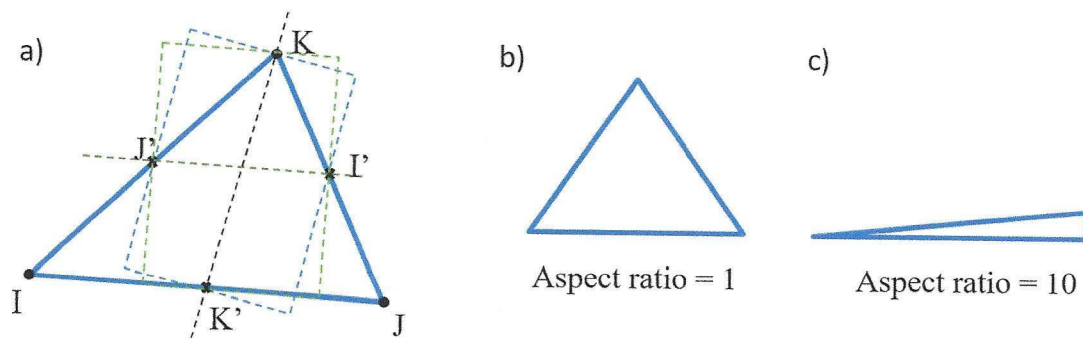


Figure 2.8: Computation of the aspect ratio for a triangle

than 165° is considered as bad shape element, large corner angles may degrade the solution performance. Figure 2.9 shows a triangle with a good (60°) and bad (165°) quality.

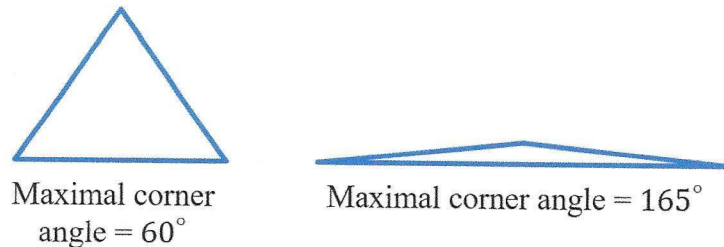


Figure 2.9: Example of triangles with different maximal corner angles.

The aspect ratio and the maximal corner deviation of a tetrahedra is computed using the definition of the same measure on a triangle. The element ~~shape~~ parameter is assigned as the worst value over the triangles defined by the tetrahedra's faces and cross-sections.

Skewness

The skewness of a triangular element is computed using the equivalent volume deviation method. It is defined as the difference between the optimal and real cell size over the optimal cell size. The optimal size is the size of an equilateral cell with the same circum radius. According to its definition, the value of 0 indicates an ideal cell, from 0 to 0.75 the cell is considered to have a good quality, from 0.75 to 1 the cell is considered to have a bad quality and a value of 1 indicates a completely degenerated cell (Figure 2.10).

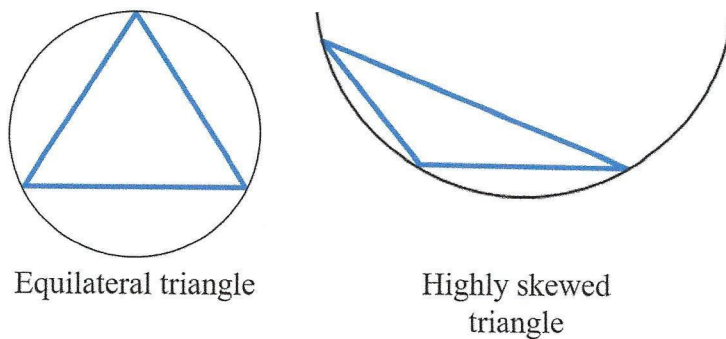


Figure 2.10: Example of triangles with different skewness with the corresponding circum radius.

2.3 Contact mechanics

In order to transfer the loads between elements, the nodes have to be connected together. If two bodies are separated with no common nodes, no interaction will occur during the deformation and the bodies will pass through each other. Here, an asymmetric surface-to-surface contact method is used to solve the multi-body interaction problems.

Let's consider two different bodies \mathcal{A} and \mathcal{B} and their occupied domains Ω_A and Ω_B with boundaries Γ_A and Γ_B respectively (see Figure 2.11). Also, we note Ω the domain of intersection of two bodies. The contact interface is the intersection of the surfaces of the two bodies:

$$\Gamma = \Gamma_A \cap \Gamma_B.$$

The intersection consists of two surfaces, usually distinguished as **target** and **contact** surfaces. For an asymmetric contact each surface has a single designation and the choice of the surface type is made following these next guidelines (the target surface property are enumerated in their priority order):

- 1035 • if the body \mathcal{A} is stiffer than the body \mathcal{B} , the surface Γ_A defines the target and Γ_B the contact surface.

- if Γ_A is a concave surface getting in contact with the convex surface Γ_B , the surface Γ_A defines the target and Γ_B the contact surface.

- if ~~the surface~~ Γ_A is larger than Γ_B , the surface Γ_A denotes the target and the Γ_B the contact surface.

For the following, we identify Γ_A as the target surface and Γ_B as the contact surface (Figure 2.11).

Sometimes, the asymmetric contact does not perform satisfactory results and a symmetric contact is needed. When defining a symmetric contact, each surface coming in contact is designated to be both contact and target surface type. Therefore, two set of contact

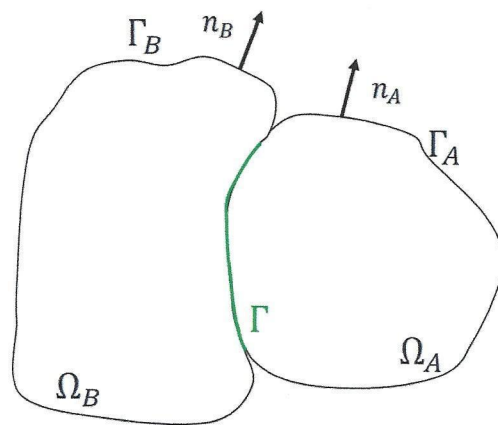


Figure 2.11: Multi-body contact problem.

When

pairs are defined. The symmetric contact may be used when the distinction between the contact and the target surfaces is not clear or to reduce the contact penetration. However it usually results in a more time-consuming solution.

~~additional~~ 2.3.1 Contact interface equations ~~besides~~

- ¹⁰⁵⁰ In the case of multi-body interaction, ~~in addition to~~ the standard mechanical governing equations, two ~~more~~ contact conditions have to be fulfilled: the two bodies cannot inter-penetrate and the traction must satisfy momentum conservation on the contact interfaces.

Traction conditions

- ¹⁰⁵⁵ Traction conditions must follow the balance of momentum across the contact interface:

$$t_A + t_B = 0 \quad (2.35)$$

On the contact boundary surface Γ , the traction vector is decomposed into its normal and tangential components:

$$t_A^n = t_A \cdot n_A, \quad t_B^n = t_B \cdot n_B$$

$$t_A^t = t_A - t_A^n n_A, \quad t_B^t = t_B - t_B^n n_B$$

Therefore the momentum balance requires:

$$t_A^n + t_B^n = 0, \quad t_A^t + t_B^t = 0 \quad (2.36)$$

Inter-penetrability condition

- 1060 The bodies implied in a multi-body problem must fulfill the inter-penetrability condition:

$$\Omega_A \cap \Omega_B = 0 \quad (2.37)$$

Decomposing the displacement u into its normal and tangential components u^n and u^t respectively the inter-penetrability condition can be written as:

$$t^n \leq 0, \quad u^n - gn_a \leq 0, \quad t^n(u^n - gn_a) = 0 \quad (2.38)$$

Where g is the gap between the two bodies and n_a is the normal to the target surface.

2.3.2 Surface interaction models

- 1065 When two solid bodies are placed together under a nonzero normal force and acted upon by another with a tangential force, a **friction force** $f_{friction}$ tangential to the interface and opposite to the applied force is created. Depending on whether the applied force can overcome the friction force opposing it, the bodies may or may not move relative to each other. The body motion along the interface is called **sliding**. The **sliding force**, $f_{sliding}$ is the applied tangential force which causes the sliding motion between the two bodies.

- 1070 Determining whether relative motion will or will not occur requires balancing the involved forces. According to the allowed relative body motion in tangential or normal directions, five types of surface interaction models are distinguished: bonded, rough, no-separation, frictional and frictionless. Table 2.1 resumes each corresponding mechanical behavior. If the body motion is not allowed in normal or tangential direction once the bodies get in contact, the respective components of traction are equals ($t_A = t_B$), which means that, for a pure **bonded** contact, the two bodies are considered as a unique solid body.

Name	body motion in normal direction	body motion in tangential direction
Bonded	No	No
Rough	Yes	No, $f_{friction} \gg f_{sliding}$
No-separation	No	Yes, $f_{friction} = 0$
Frictionless	Yes	Yes, $f_{friction} = 0$
Frictional	Yes	Yes, if $f_{sliding} > f_{friction}$

Table 2.1: Surface interaction models and corresponding mechanical behaviors

- 1080 The *frictional* contact behavior is defined using Coulomb friction law. For a continuous body the Coulomb friction model is applied at each point of the contact interface. Considering that bodies \mathcal{A} and \mathcal{B} are in contact within the surface Γ , then for all $x \in \Gamma$:

$$\text{if } \|t^t(x)\| < -\mu_f t^n(x), \quad \Delta u^t = 0 \quad (2.39)$$

lower than

$$\text{if } \|t^t(x)\| = -\mu_f t^n(x), \quad \Delta u^t = -k(x)t^t(x), \quad k(x) > 0 \quad (2.40)$$

Where μ_f is the material property named **friction coefficient**, Δu^t is the slip incremental in the tangential direction and $k(x)$ is a variable computed from the momentum equation. The condition 2.39 is known as the sticking condition: the tangential traction is less than the critical value, thus no sliding occurs. Reciprocally, condition 2.40 is called the sliding condition.

When a frictionless contact model is used, $\mu_f = 0$, the tangential tractions vanish completely: $t_A^t = t_B^t = 0$. On the contrary, when a rough contact is modeled, the friction coefficient μ_f is equal to infinity, so that the sticking condition is always fulfilled.

In practice, several contact models can be combined to model a physical contact between two bodies.

2.3.3 Contact formulation algorithm: pure penalty model

1095 Pinball region

Contact formulation presents two primary difficulties from a computational point of view. First, the traction conditions have to be estimated for each considered frictional model. And second, ~~is the unpredictability of regions which will get in contact with each other during the deformation process~~ *can not be predicted*.

1100 The region of contact depends on materials properties and imposed boundary conditions, therefore, it is difficult to know a priori where the surfaces will be in contact. To formulate analytic equations, one has to know exactly the nodes involved in the contact process. Therefore, during body deformation, the program calculates if the contact is *opened* or *closed*. The status is defined using a sliding pinball (Figure 2.12). The pinball slides over the contact surface nodes and searches for the target surface. If the node to surface distance is smaller than the pinball radius, the contact is considered to be closed (Figure 2.12, green nodes), otherwise the contact is considered to be opened (Figure 2.12, gray nodes).

Gap and penetration measures

belonging

1110 Let's consider a point x_B belonging to the body surface Γ_B and x_A the intersection point of the surface normal n_B with the surface Γ_A (Figure 2.13). The point to surface distance $d_1(x_B, \mathcal{A})$ is defined as:

$$d_1(x_B, \mathcal{A}) = \|x_B - x_A\| = \left[\sum_{i=1,2,3} (x_B^i - x_A^i)^2 \right]^{\frac{1}{2}} \quad (2.41)$$

If the intersection point x_A is located inside the pinball area, the node to surface distance define the amount of **gap** or **penetration** of the respective node (Figure 2.13).

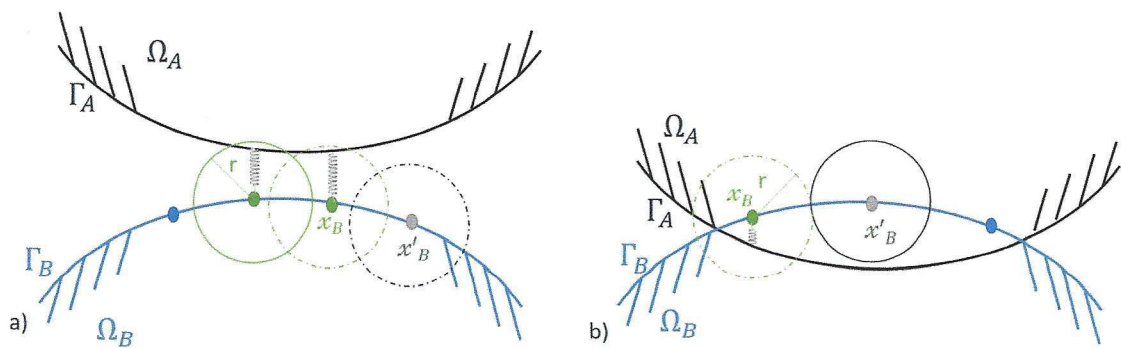


Figure 2.12: Contact status update using a pinball of radius r . Green nodes - updated nodes to closed contact status; gray nodes - updated nodes to open contact status; blue nodes - nodes which contact status need to be updated

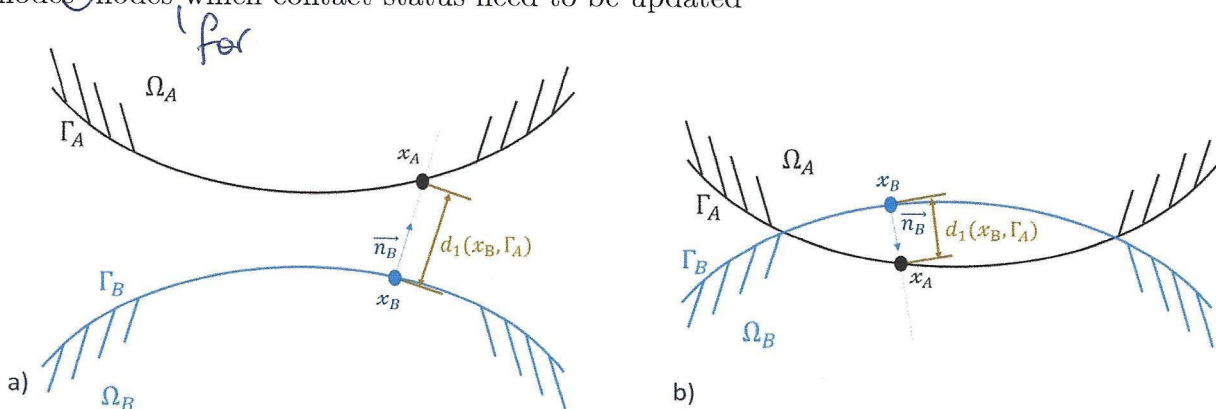


Figure 2.13: a) Body \mathcal{A} and body \mathcal{B} are close but not in contact. The $d_1(x_B, \mathcal{A})$ measure defines the gap between the bodies at point x_B . b) Body \mathcal{B} have penetrated the body \mathcal{A} . The $d_1(x_B, \mathcal{A})$ measure gives the penetration at point x_B .

Computing the gap or penetration at single points increases numerical instabilities. Therefore, in this work, the gap and penetration are computed in an averaged manner over the projected surface areas. Figure 2.14 shows the projected surface areas (c) obtained by the intersection of the target surface areas (a) with the projected contact surface areas (b) over the target areas (a). [Il manque une conclusion.]

The interested reader is referred to ANSYS contact technology guide (ANSYS, 2017a) for more details on the contact modeling.

Finite element mesh

For the finite element computation, contact and target surfaces have to be discretized with 2D linear or quadratic elements (Figure 2.7) consistent with the underling 3D element

[J'ne comprend pas ce qu'il appelle la figure 2.14 ?]

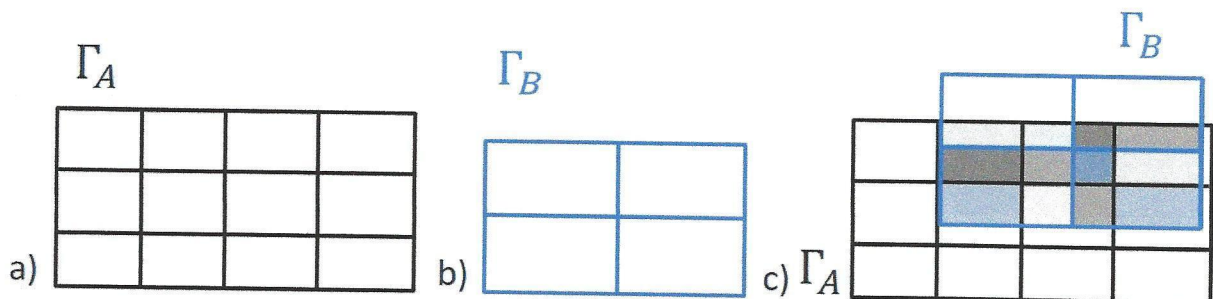


Figure 2.14: The contact surface projection over the target surface: a) Target discretized area; b) contact discretized area; c) intersection of the projected surfaces.

mesh. The elements are named contact and target elements respectively. They have no material properties apart the friction coefficient μ_f . The stress-strain as well as the gap or penetration measures are computed for each mesh node of the discretized surface.

¹¹³⁰ **Pure Penalty method**

In this manuscript, one of the most popular mathematical expression of contact compatibility conditions is used, namely the penalty method. With such a method, additional contact properties are defined to manage contact behavior: a normal stiffness factor, opening stiffness factor, and a tangential stiffness factor. Such factors play an important role ¹¹³⁵ in the numerical computation but have no physical meaning.

The penalty method uses a spring like relationship to introduce a force for all nodes pairs (contact-target) that are defined to be in closed contact (Figure 2.41). The contact force is computed using the following expression:

$$f_c = k_c d \quad (2.42)$$

where d represents the penetration or gap amount and k_c is the normal stiffness factor ¹¹⁴⁰ or the opening stiffness factor respectively. The tangential stiffness factor works in the same way enforcing the responding frictional force. Even if physical contacting bodies do not interpenetrate ($d = 0$), some finite amount of penetration, $d > 0$, is required mathematically to maintain equilibrium.

The biggest challenge here is that the magnitude of the stiffness contact factors is completely unknown beforehand. The contact force at each node have to be large enough to push the contact surface back to the target surface and eliminate unwanted penetration or gap. ¹¹⁴⁵ At the same time, if the contact force is too large, it pushes the contact surface far away from the pinball region causing error and solution instabilities.

2.4 Breast biomechanical model: overview

Biomechanical modelling of breast tissues has been widely investigated for various medical applications such as surgical procedure training, pre-operative planning, diagnosis and clinical biopsy, image guided surgery, image registration, and material parameter estimation (Table 2.3). For the last 20 years, several research groups have presented their breast models based on finite elements modeling. The complexity and relevance to breast anatomy of each model depend on the research purposes for which it was designed.

Several groups have proposed biomechanical breast models to register uncompressed volumetric breast data to the compressed one (Han et al., 2012; Ruiter et al., 2006; Sturgeon et al., 2016) or to compressed projection mammographic data (Kellner et al., 2007). Within this framework, the authors modeled the breast deformation from prone to compressed prone position assuming linear elastic materials, zero residual stress and Dirichlet boundary conditions. However, compression-like breast deformation is too limited to characterize global breast mechanics.

Applications such as image guided surgery or preoperative planning imply a wider range of deformations. Therefore biomechanical breast models capable of estimating gravity induced deformation between different body positions were proposed, for example from supine to prone positions (named also multi-loading gravity simulations) (Gamage et al., 2012; Georgii et al., 2016; Eiben et al., 2016c). Considering the involved large deformation, these models need to be more accurate with respect to mechanical and anatomical breast properties. In this respect, a patient-specific model is needed considering more personalized boundary conditions, material models and a better representation of breast anatomy.

As described in Section 2.1, to build such a mechanical breast model, one needs to provide the breast geometry in a **reference configuration**, the **constitutive models** of tissues composing the volume and the **boundary conditions**. The definition of all these variables has a significant impact on model accuracy.

2.4.1 Breast reference configuration

A large number of existing patient specific models are using volumetric data from MR images (Carter (2009b), Kellner et al. (2007), Conley et al. (2015), Eiben et al. (2016b), Martínez-Martínez et al. (2017)) or CT images (Palomar et al. (2008), Sturgeon et al. (2016)) to design the breast geometry. During such exams, the acquired breast tissues are already deformed with deformations that significantly change breast geometries, for example if the patient is in a supine or in a prone position. Moreover, the deformed breast configurations include already the initial pre-stresses which are generally unknown and are extremely difficult to measure in clinical conditions.

To model the breast tissues deformation under gravity loading, the reference state is chosen to be the breast geometry in a stress-free configuration, i.e. without being deformed by any force, including gravity. The breast stress-free geometry is practically impossible to measure; therefore, several estimation methods have been proposed. The four most used

ones are described below.

Methods

Inverse gravity

1190 (Palomar et al., 2008; Sturgeon et al., 2016) used the inverse gravity method to estimate the stress-free geometry from the prone position measured during the exam. In their work, the authors just reversed the gravity effects without considering the initial stresses already included in the breast prone configuration. According to Eiben et al. (2014) the inverse gravity methods gives a poor approximation of the breast reference state and can be used only with small deformations or highly constrained models.
1195

Breast neutral buoyancy configuration

Assuming that breast density is equal to water density, Rajagopal et al. (2008) compute the breast stress-free configuration by imaging the breast immersed in water. Following the same physical assumptions, Kuhlmann et al. (2013) proposed to estimate the stress-free 1200 configuration by applying a hydro-static distributed load on the breast surface collected in a prone configuration. Even though the estimated geometries are accurate enough, these methods are time-consuming and are difficult to transpose in a clinical framework.

Prediction-correction iterative algorithm

The prediction-correction iterative method was first proposed by (Govindjee and Mihalic, 1205 1998) and adapted later by Carter (2009b) and Eiben et al. (2014). The original method is based on the prediction-correction iterative scheme represented in Figure 2.15. The first approximation of the breast reference configuration is estimated by applying the inverse gravity method on the prone breast configuration (see above). Then, a numerical breast prone configuration is computed and compared to the corresponding measured one. The 1210 difference between the two prone geometries (The measured one and the simulated one) is used to update the reference breast configuration. The process is repeated until the convergence is achieved (i.e. then the difference is minimal). These methods were validated using the neutral buoyancy breast shape.

Inverse FE algorithm

Pathmanathan et al. (2008) and later Vavourakis et al. (2016) proposed an analytic computation of the breast reference state by reparametrizing the equilibrium equation and by solving a finite element formulation of the inverse motion. The model provides good estimates of breast reference configurations but needs large numerical resources. Eiben et al. (2014) showed that the prediction-correction iterative algorithm and the inverse FE 1215 1220 algorithm are similar in terms of resulting accuracy.

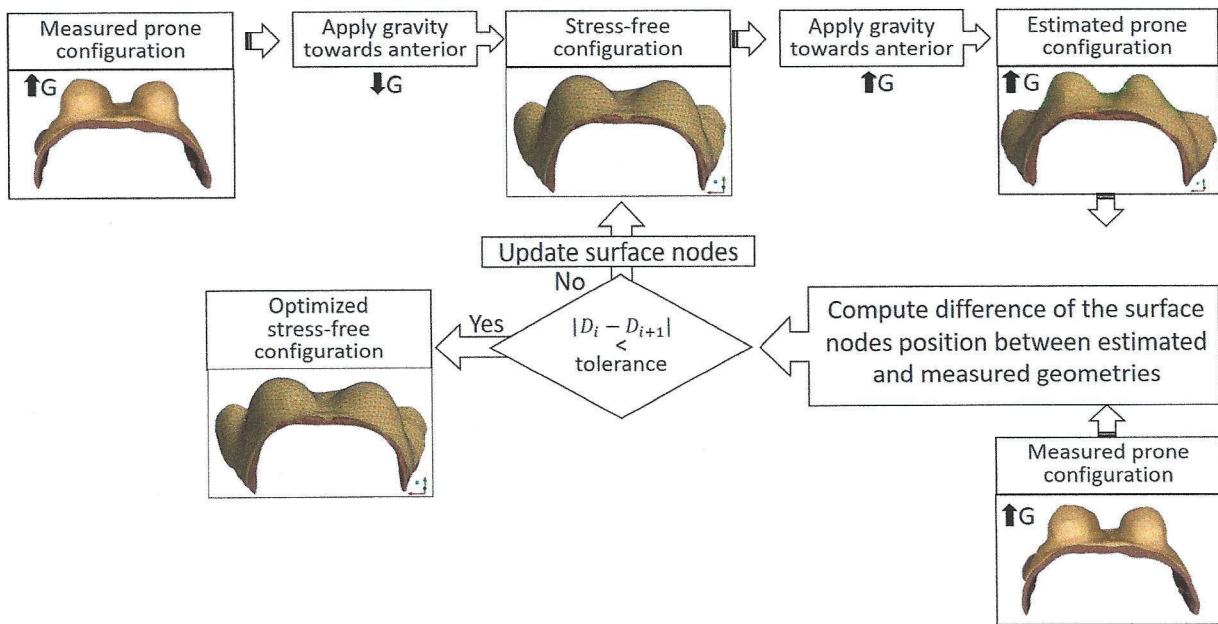


Figure 2.15: Prediction-correction algorithm

2.4.2 Constitutive models

fluid (blood and lymph)

Global breast mechanics is governed by breast tissue compositions and their individual mechanical properties. The breast soft tissues are known to be incompressible, nonlinear, anisotropic, and viscous materials. However, according to Wellman et al. (1999) the breast tissues viscosity can be neglected even when short time scales loads are applied.

Under large compression and body position changes, the breast volume can vary due to blood flows. Thus, soft tissues are frequently modeled as quasi-incompressible materials with a Poisson ratio ranging between $\nu = 0.45 - 0.5$. The influence of the Poisson ratio within linear constitutive models was studied for breast by Tanner et al. (2006); according to the authors, the best estimates are obtained with high Poisson ratio ($\nu = 0.495, 0.499$). The breast tissues are predominately composed of water; therefore, the density is considered to be equal to 981 kg/m^3 .

For the last decades several constitutive models were used to model the breast tissues response to an external force: exponential elastic (Azar et al., 2002), Neo-Hookean hyperelastic (Carter, 2009b; Rajagopal et al., 2010b; Sturgeon et al., 2016; Eiben et al., 2016a; Han et al., 2014; Garcia et al., 2017), Mooney-Rivlin (Samani et al., 2007; Tanner et al., 2006; Carter et al., 2012; Martínez-Martínez et al., 2017). Eder et al. (2014) compared the most popular models in a multi-loading gravity simulation; according to the authors, the Neo-Hookean model proposed by Rajagopal et al. (2008) gives the best estimates.

1240 **Glandular and adipose tissues biomechanical properties**

Multiple studies have shown that breast composition, and so its mechanical behavior undergo substantial changes during woman lifetime (section 1.1.4). The first studies on mechanical proprieties estimation of breast tissues were done in diagnosis purposes. When the breast is developing benign or malign disorders, its mechanical properties differ from the ones of the normal breast tissues. In a study of 142 samples, belonging to 4 type of tissues, Krouskop et al. (1998) found that depending on the pre-compression level, Young moduli of invasive carcinoma is from 5 to 25 times larger than the one of normal adipose tissue (from 5% to 20% strain levels).

Later, several research groups (Table 2.2) have studied the elastic moduli of adipose and glandular tissues. The breast tissues elastic parameters range between 0.1 kPa and 271.8 kPa. Such huge variation may be explained by the differences in the experimental set-up used to estimate stiffness, but also by the participant's physical condition, age or period of the menstrual cycle. For example, Han et al. (2012), though using the same FE method, found significantly inter-individual variability, with the shear modulus ranging between 0.22 and 43.64 kPa. Lorenzen et al. (2003) showed that during the menstrual cycle, due to the hormonal changes, the elastic properties of the glandular tissues can change by about 30%.

An important difference in estimated values of breast elastic moduli is observed between the linear elastic and hyperelastic models. If only in-vivo studies with Neo-Hookean material models are considered, the range of the adipose and glandular shear moduli is significantly lower than 50 kPa.

Carter (2009b) compared a one-parameter Neo-Hookean potential function with a five-parameters Mooney-Rivlin potential function for various material properties. The multi-loading gravity simulations were thus performed on 3 subjects. According to the authors, even for parameters 10 times softer than the literature (Samani et al., 2001), the Mooney-Rivlin model underestimates the tissues deformation by at least 75% when the subject is re-positioned from the supine to the prone positions. The best estimates were given by the Neo-Hookean model with the initial shear modulus equal to 0.2 kPa.

Previously listed researches clearly showed the variability of elastic moduli of the same tissue between and within individuals. Eder et al. (2014) made a larger analysis including all material models proposed in the literature. According to authors, many of them are too stiff permitting not enough deformation within the gravity loading. This study has shown that the most reliable elastic moduli values are the ones given by Rajagopal et al. (2008) (Table 2.2).

1275 **Muscle biomechanical properties.**

Muscle is a kinematically, geometrically, and materially complex tissue. Muscle mechanical behavior depends on its contractile active and passive elastic properties (Nordez and Hug, 2010). In biomechanics the muscle is modeled using complex models as Hill-type models (Zajac, 1989), Feldman's lambda model (Feldman, 1986) which are considering the vari-

Ex-vivo estimation				
Author	Method	Material model	material properties	
			Adipose kPa	Glandular kPa
Krouskop et al. (1998)	Indentation-5%	Linear elastic	$\lambda = 19 \pm 7 \text{ kPa}$	$\lambda = 33 \pm 11 \text{ kPa}$
Krouskop et al. (1998)	Indentation-20%	Linear elastic	$\lambda = 20 \pm 6 \text{ kPa}$	$\lambda = 57 \pm 19 \text{ kPa}$
Wellman et al. (1999)	Indentation - 5%	Linear elastic	$\lambda = 6.6 \text{ kPa}$	$\lambda = 33 \text{ kPa}$
Wellman et al. (1999)	Indentation - 15%	Linear elastic	$\lambda = 17.4 \text{ kPa}$	$\lambda = 271.8 \text{ kPa}$
Azar et al. (2002)	Indentation	Exp. elastic	$b = 4.46 \text{ kPa}; m = 7.4$	$b = 15.1 \text{ kPa}; m = 10$
Samani and Plewes (2004)	Indentation	Linear elastic	$\lambda = 3.25 \pm 0.91 \text{ kPa}$	$\lambda = 3.24 \pm 0.61 \text{ kPa}$

In-vivo estimation				
Van Houten et al. (2003)	MRE	Linear elastic	$\lambda = 17 - 26 \text{ kPa}$	$\lambda = 26 - 30 \text{ kPa}$
Sinkus et al. (2005)	MRE	Visco-elastic	$\mu = 2.9 \pm 0.3 \text{ kPa}$	
Rajagopal et al. (2008)	MRI-FEM	Neo-Hookean	$\mu = 0.16 \text{ kPa}$	$\mu = 0.26 \text{ kPa}$
Carter (2009a)	MRI-FEM	Neo-Hookean	$\mu = 0.25 \text{ kPa}$	$\mu = 0.4 \text{ kPa}$
Han et al. (2012)	MRI-FEM	Neo-Hookean	$\lambda = 1 \text{ kPa}$	$\lambda = 0.22 - 43.64 \text{ kPa}$
Gamage et al. (2012)	MRI-FEM	Neo-Hookean	$\mu = 0.1 \text{ kPa}$	
Griesenauer et al. (2017)	MRI-FEM	Hooke's law	$\lambda = 0.25 \text{ kPa}$	$\lambda = 2 \text{ kPa}$

Table 2.2: Material properties for adipose and glandular tissues.

1280 ation of muscle elasticity in function of muscle state. In breast biomechanical models the muscle is combined with the thoracic cage and is frequently considered as a rigid breast support. In most of models, the pectoral muscle is modeled by imposing zero-displacement conditions on nodes closer to the chest wall (Samani et al., 2001; Chung et al., 2008; Rajagopal et al., 2010a) or by allowing them to slide along the chest wall line (Han et al., 1285 2014; Georgii et al., 2016).

The muscle is nonlinear, anisotropic, incompressible material. The bibliographic data on static mechanical properties of the muscle-tendon unit assessed by supersonic shear wave imaging elastography state a Young's modulus in range of 20kPa to 300kPa depending on

CHAPTER 2. BIOMECHANICAL BREAST MODELING STATE OF THE ART

the muscle location and subject's physical condition (Lima et al., 2018). The muscle shear moduli on the upper trapezius was studied by Leong et al. (2013), according to authors the muscle shear elasticity at rest was $17.11 \pm 5.82 \text{ kPa}$, and this increased to $26.56 \pm 12.32 \text{ kPa}$ during active arm holding at 30 degrees abduction.

Skin biomechanical properties

Several studies have shown the importance of skin in biomechanical breast modeling. According to Carter (2009b), a model which includes the skin estimates better the tissues deformation under gravity loading.

(Sutradhar and Miller (2013) published a complete study of breast skin estimating its elasticity for 16 different breast regions. The study was done on 23 female volunteers aged from 29 to 75 years. The authors found that the skin elastic moduli range between 15 ~~to~~ 480 kPa with an average of $334 \pm 88 \text{ kPa}$. The elastic moduli in the lateral region (mean 370 kPa) has the highest value followed by the superior region (mean 355 kPa), the inferior region (mean 331 kPa) follows next, with the medial region having the lowest value (mean 316 kPa). However, no significant variation of elastic moduli in radial direction was found.

Other researches on skin elasticity are available, but they are not specific to the breast skin. Hendriks et al. (2006) estimated in-vivo skin properties by suction testing. The skin was considered as a homogeneous, isotropic, incompressible, hyperelastic material. The study was performed on 14 subjects and the obtained average of elastic moduli for skin was 58.4 kPa.

The estimation of the breast skin elasticity by the means of finite elements using Neo-Hookean potential function has resulted in softer materials model. Carter (2009a) found an initial shear modulus equal to 16 kPa, whereas Han et al. (2014) found that for the five studied subjects the skin shear moduli ranged between 2.47 kPa and 5.78 kPa.

Fascias and ligaments biomechanical properties

The surrounding breast fascias and the supervisory ligament form the breast support matrix. These structures are well described for surgical purposes (thickness, location etc), however little is known about their mechanical properties. The first biomechanical breast model taking into account the effect of Cooper's ligaments was proposed by Azar et al. (2002) and took up later by Pathmanathan et al. (2008) and Han et al. (2012).

The authors designed a new material model for fatty tissues including the anisotropic behavior of breast ligaments. Later, Georgii et al. (2016) come up with a spring-mass generic model for the breast support matrix. According to the authors, including the ligaments into the finite elements breast model have increased the robustness of the prone-supine simulation with respect to the input parameters.

To our knowledge, there are no experimental data describing the mechanical properties of breast superficial fascia. An approximation of the elastic moduli of Cooper's ligaments is given by Gefen and Dilmoney (2007) by extrapolating from known ligamentous structure provided

52 pour tout à mémoire

available in the literature

Draft

REMARQUE GÉNÉRALE: J'aînerais que tu changes les phrases telles que " Sutradhar and Miller (2013) published a complete study..." en " A complete study was performed (Sutradhar and Miller, 2013)." Une référence doit voter une référence et ne pas être utilisée comme un morceau de phrase (sujet p.ex.).

ranging and modulus
in the human body. The authors estimated the elastic moduli of suspensory ligaments to relay between $80 - 400 \text{ MPa}$

1330 Fibrous tissues get their elasticity from elastin elastic fibers and their structural support from collagen fibers. As reported by Riggio et al. (2000), the superficial fascia is made up of both collagen and elastin fibers. In contrast, the Cooper's ligaments appeared to be composed almost of collagen fibers. The mechanical properties of a single collagen fiber from a rat tail were studied by Wenger et al. (2007); according to the authors the corresponding elastic moduli range between 5 GPa and 11 GPa . Other studies on biomechanical characterization of human body superficial fascia are available in the literature. The most frequently studied structures are the plantar fascia and foot ligaments, with a Young's modulus ranging between $0.1 \text{ e}^{-3} \text{ MPa}$ (Gefen, 2003) and 700 MPa (Cheung et al., 2004).

2.4.3 Boundary conditions

1340 Dirichlet conditions are usually used to constrain the sternum/axilla ends and the posterior surface of the breast or the thoracic cage if the muscular tissues are considered (Griesenauer et al., 2017; Rajagopal et al., 2008; Pathmanathan et al., 2008; Gamage et al., 2012; Griesenauer et al., 2017). As reported by Carter (2009b) the zero-displacement boundary conditions in a multi-gravity loading framework result in an over-constrained model, in that case sliding conditions on the mesh nodes corresponding to the chest wall have to be considered.

1350 Later, several teams using biomechanical breast models for multy modality image registration or surgical planing showed that including the sliding boundary conditions (Georgii et al., 2016; Han et al., 2014) improves the registration accuracy. However the most studies in which the biomechanical model is designed for breast compression, the tissues sliding over the chest wall is neglected and fixed boundary conditions are usually assumed (Sturgeon et al., 2016; Martínez-Martínez et al., 2017).

2.4.4 Summary

1355 During the last decades, several breast biomechanical models were proposed. However, only a small part of them (Carter, 2009b; Gamage et al., 2012; Han et al., 2014) were evaluated with respect to real tissues deformations. As we intend to build-up a subject specific breast biomechanical model capable of estimating multi-loading gravity deformations, we will only consider as relevant the biomechanical models that were evaluated and compared with real data. In this chapter, three biggest challenges were identified: the estimation of the breast reference geometry, the estimation of patient specific material properties and the definition of the boundary condition and namely the breast-muscle interface. Today's outstanding breast biomechanical models are represented by the next three models: Eiben et al. (2016c), Han et al. (2014), Gamage et al. (2012).

1365 Gamage et al. (2012) proposed a finite elements model capable to estimate the supine breast configuration from the prone one. The breast stress-free configuration was estimated using a prediction-correction iterative algorithm optimization process, in this purpose the

skin surfaces on prone configuration was used as ground-truth. Contrariwise, the material constitutive parameters were identified using the skin surface on supine breast configuration by applying a non-linear optimization algorithm. Breast tissues sliding over the chest wall was considered partially by modeling the pectoral muscle as a soft structure and including it into the optimization process. The models were evaluated for the supine breast configuration by computing the root-mean-squared error (RMSE) from the point to surface distance between the estimated and measured data. Conform to the authors, the breast supine geometry was estimated within an RMSE of 5mm (maximal distance of 9.3 mm).

1375 [laterson,

In the same time, Han et al. (2014) developed a breast biomechanical model for image registration. The estimates of supine breast configuration were computed for five subjects, and the accuracy was assessed by computing the Euclidian distance between anatomical landmarks. The mean Euclidian distance ranged between 11.5 mm and 39.2 mm (maximal Euclidian distance ranged between 20.3mm and 61.7mm). The authors modelled the elongation of the pectoral muscle using a contact sliding model. Only the material constitutive parameters were adapted to the patient's breast mechanics, the stress-free breast geometry being estimated by inverse gravity.

Finally, Eiben et al. (2016c) proposed a new model to estimate the up-standing breast configuration from the prone one. The model was evaluated on 3 subject. The patient specific stress-free geometry was computed using an inverse finite elements u-p formulation. The material parameters were optimized such that the best fit in supine configuration is obtained. The estimates quality was measured in terms of the mean Eulerian Distance between manually selected internal landmarks. Thus, the supine breast configuration was estimated within a mean distance ranging between 12.2mm and 19.8mm. The model evaluation for the up-standing configuration was not presented.

A new biomechanical breast model is proposed in the next chapter considering the patient specific breast geometry and elastic properties as proposed by the previous models. In addition, the breast tissues sliding over the chest wall is modeled by including new anatomical structures as superficial fascia and suspensory ligaments. We believe that global breast mechanics are driven by these stiff structures. Finally, the model will be evaluated by confrontation with real data collected from MR images.

such behavior is

However, (In the next chapter, a new biomechanical model of the breast will be described. We propose this model

Authors	Application	FE mesh	Material models	Boundary conditions	Stress-free config.
Azar et al. (2002)	Computer assisted breast surgery	8-Node hexahedrons (trilinear isotropic elements)	Skin-elastic adipose,glandular-hyperelastic polynomial	Sliding between breast - thorax and breast-paddle	Prone breast geometry
Rajagopal et al. (2007)	Breast compression	8-Node hexahedrons (tricubic Hermite elements)	Homogeneous , Neo-Hookean model	Zero-displacement BC	Buoyant breast in water
Pathmanathan et al. (2008)	Image registration	8-Node hexahedrons (trilinear elements)	Homogeneous polynomial Skin exponential hyperelastic	Zero-displacement on muscle; Compression with imposed displacement	Inverse FE algorithm
Han et al. (2014)	Image registration	4-Node tetrahedrons	Muscle, glandular, fatty, skin - Neo-Hookean model	Sliding on pectoral muscle	Inverse gravity
Gamage et al. (2012)	Computer assisted breast surgery	8-Node hexahedrons (tricubic elements)	Homogeneous+ Neo-Hookean incompressible model	Zero-displacement BC on rib cage surface, Sternum, axilla ends, shoulder	PC iterative algorithm
Patete et al. (2013)	Computer assisted breast surgery	4-Node tetrahedrons (trilinear isotropic elements)	Adipose , glandular, skin	Zero-displacement BC on the chest wall	PC iterative algorithm
Kuhlmann et al. (2013)	image registration	4-Node tetrahedrons	Adipose, glandular-linear gel-like (Eulerian formulation); Skin - hyperelastic material (Lagrangian formulation)	Zero-displacement chest wall	PC iterative algorithm
Georgii et al. (2016)	Surgery simulation	8-Node hexahedrons, 2-node 3D spars	homogeneous elastic material, Cooper's ligaments-generic mass-spring model	sliding BC (breast on the pectoral muscle)	NA
Eiben et al. (2016c)	Surgery outcome prediction	4-Node tetrahedrons	Fatty , Hookean model; skin-exponential hyperelastic	Zero-displacement BC	Inverse FE algorithm
(Garcia et al., 2017)	3D breast lesion localization	4-Node tetrahedrons	adipose, glandular - Neo-Hookean models	zero-displacement BC	Prone breast configuration

Table 2.3: Breast biomechanical models